Verification of scaling behavior near dynamic phase transitions for nonantisymmetric field sequences

M. Quintana [*] and A. Berger
CIC nanoGUNE BRTA, E-20018 Donostia-San Sebastián, Spain

(Received 31 January 2024; accepted 11 April 2024; published 10 May 2024; corrected 26 June 2024 and 7 August 2024)

We investigate the scaling behavior of the magnetic dynamic order parameter Q in the vicinity of the dynamic phase transition (DPT) in the presence of temporal field sequences $H(t)$ that are periodic with period P but lack half-wave antisymmetry. We verify by means of mean-field calculations that the scaling of Q is preserved in the vicinity of the second-order phase transition if one defines a suitable generalized conjugate field H^* that reestablishes the proper time-reversal symmetry. For the purpose of our quantitative data analysis, we employ the dynamic equivalent of the Arrott-Noakes equation of state, which allows for a simultaneous scaling analysis of the period P and the conjugate-field H^* dependence of Q. By doing so, we demonstrate that both the scaling behavior and universality are preserved, even if the dynamics is driven by a more general applied field sequence that lacks antisymmetry.

DOI: 10.1103/PhysRevE.109.054112

I. INTRODUCTION

Phase transitions are one of the most remarkable phenomenon in many-body physical systems given that they exhibit an abrupt qualitative change of an associated order parameter upon modifying an external control variable, such as temperature, for instance. While originally associated with thermodynamic equilibrium physics, phase transitions can also be found in systems that are far from equilibrium upon changing the driving force of the associated nonequilibrium dynamics [1,2]. These nonequilibrium phase transitions have been documented in a wide variety of physical systems such as superconducting materials [3,4], brain activity [5], or charge-density waves [6,7]. Their understanding and their analogies with conventional thermodynamic phase transitions (TPTs) make them crucially relevant phenomena in nonequilibrium physics [8,9]. This is particularly true in the context of the critical scaling behaviors of the associated order parameters. Indeed, some of these dynamical systems are known to exhibit Ising-like criticality, even if they are far from thermodynamic equilibrium conditions, which makes them particularly interesting systems for the purpose of investigating analogies between equilibrium and nonequilibrium phase transitions [10,11].

A particularly important type of nonequilibrium phase transition is the dynamic phase transition (DPT) of ferromagnets. The DPT is known to occur in ferromagnetic (FM) systems at temperatures below the Curie temperature T_C, and its relevance is associated with the fact that it has substantially contributed to the general understanding of nonequilibrium phase transitions [12,13]. At the DPT, the dynamic magnetization behavior $M(t)$ exhibits abrupt changes when varying a time-dependent oscillating magnetic field of given amplitude H_0 and period P, which represent the external control parameters. An understanding of the DPTs in ferromagnets was initially advanced by theoretical work utilizing mainly kinetic Ising-like models [14–16]. In such models, a ferromagnet is typically described by localized spin-½ systems with nearest-neighbor exchange interactions of coupling strength J, and a relaxation time constant τ, with which M approaches its equilibrium value upon abruptly changing the external field H [12,17].

In these works, it was observed that the period-averaged magnetization

$$Q = \frac{1}{P}\int_t^{t+P} M(t')\,dt', \tag{1}$$

plays the role of the order parameter associated with the DPT. Here, Q exhibits a nonzero value in a dynamically ordered or FM phase for P below a certain critical period P_c. For $P > P_c$, the system will exhibit a disordered or paramagnetic (PM) phase with $Q = 0$ and, accordingly, it was found that P_c defines the critical period at which the system exhibits a second-order phase transition (SOPT) [12].

Figures 1(a) and 1(b) show exemplary $M(t)$ trajectories corresponding to the PM and FM phases as solid red lines, respectively, in the presence of a sinusoidal field sequence $H(t) = H_0 \sin(2\pi t/P)$ for two different P values, shown as black-dotted lines [18]. Specifically, Fig. 1(a) shows the $M(t)$ behavior in slow-field dynamics, with $P/\tau = 100$, corresponding to the PM phase. Here, M exhibits a periodic reversal that is slightly delayed with respect to the field, given the coercivity of the ferromagnetic spin systems. In contrast, Fig. 1(b) shows the two equivalent stable trajectories, corresponding to the FM phase for a lower $P/\tau = 8$ value. In this case, $M(t)$ does not exhibit full magnetization switching but instead only oscillates slightly around one of the two equivalent nonzero magnetization values that corresponds to a nonzero Q, represented as green-dashed lines. The two equivalent dynamical states correspond to the bifurcation of the stable states in the magnetic phase diagram [19].

[*]Corresponding author: m.quintana@nanogune.eu

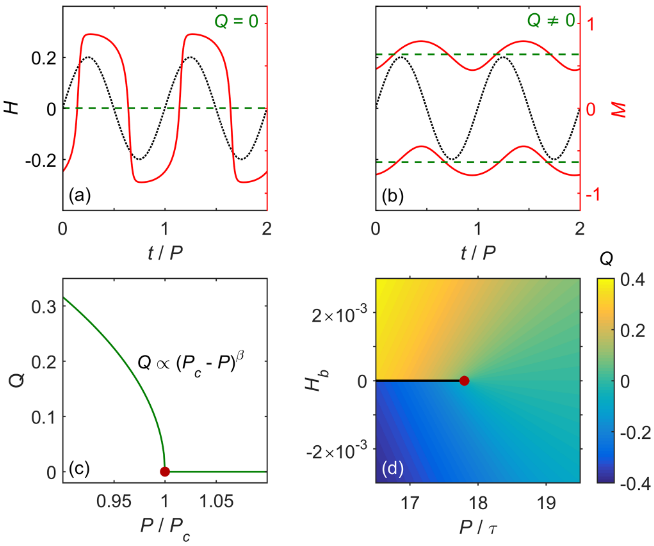

FIG. 1. (a), (b) $M(t)$ behavior, shown as solid red lines, in the presence of a sinusoidal $H(t)$ field with $H_0 = 0.2$, displayed as dotted black lines, showing the dynamic behaviors in the PM ($P/\tau = 100$) and FM ($P/\tau = 8$) phases, respectively. The green dashed lines represent the dynamic order parameter Q. (c) Q vs P, showing the SOPT at exactly P_c (dark-red point), and separating the FM and PM phases together with the scaling of Q close to P_c. (d) Color-coded map of the phase-space behavior of $Q(P, H_b)$. The central black line represents the phase line at $H_b = 0$ in the FM phase responsible for the FOPT, whereas the dark-red dot in the center represents the SOPT. The color bar is shown on the right-hand side of (d). The data shown here are the results of MFA calculations, which are discussed in conjunction with Eq. (6).

In the vicinity of P_c, Q is known to exhibit a power-law behavior as a function of P with a critical exponent β, namely [20]

$$Q \propto (P_c - P)^{\beta} \quad \text{for } P < P_c. \tag{2}$$

This behavior is formally identical to the TPT case, in which the equilibrium magnetization M exhibits scaling behavior as a function of the temperature T near T_C. Furthermore, the TPT and DPT have the same universality class and, thus, β is identical in both phase transitions, as shown both in Monte Carlo [21,22] and mean-field calculations [12,23] of the Ising model. In Fig. 1(c), we display the Q vs P dependency, showing the occurrence of the FM and PM phases, separated by a SOPT at exactly P_c, together with the critical scaling of Q as P approaches P_c.

A constant bias field H_b, superimposed to the field oscillations, was more recently confirmed to play the role of the conjugate field of Q, at least for a specific subset of $H(t)$ sequences [23–26]. This implies that in the FM phase, the system will exhibit a first-order phase transition (FOPT) upon crossing the $H_b = 0$ value. Hereby, Q will exhibit a hysteretic behavior as a function of H_b in the dynamic FM phase when the system crosses the $H_b = 0$ value, an aspect that was also verified experimentally [19]. This identification of H_b as the conjugate field has now allowed for the definition of a proper (P, H_b) phase space, in which Q is observed to exhibit both FOPT and SOPT. In Fig. 1(d), we show specifically as a color-coded map the phase-space behavior of the dynamically stable states $Q(P, H_b)$ with the first- and second-order phase transitions indicated as a solid black line and dark-red point, respectively. Here, we observe the two equivalent opposite stable FM states for $P/\tau < 17.78$, represented by the upper-yellow and lower-blue regions of the map, for which the abrupt sign change of Q is associated with the FOPT occurring along the $H_b = 0$ line. In contrast, in the PM phase, Q changes continuously as a function of H_b.

At exactly the critical point, Q is known to also exhibit scaling behavior as a function of H_b, specifically

$$Q \propto {H_b}^{1/\delta} \quad \text{for } P = P_c, \tag{3}$$

with β, $\delta = 1 + \gamma/\beta$, and γ being the relevant dynamic critical exponents [13]. These relevant scaling relations of Q in the vicinity of the critical point have been verified theoretically [20–22,24], and recently, they have also been confirmed by means of experiments on ultrathin ferromagnetic films with in-plane uniaxial symmetry [27] and specialized magneto-optical characterization techniques [28,29].

One fundamental aspect required for Eqs. (2) and (3) is the time-reversal symmetry in the entire dynamic phase space [25,26]. Such time-reversal symmetry results in an antisymmetric behavior of the stable states of Q as a function of H_b for all P, namely

$$Q(P, H_b) = -Q(P, -H_b). \tag{4}$$

This particular relationship, however, is only valid if the time-dependent field component exhibits half-wave antisymmetry, defined as $H(t) = -H(t + P/2)$ [26]. Half-wave antisymmetry implies that the even-order components in the Fourier space will be strictly null. In previous studies, it has been demonstrated that the presence of even harmonic-field components other than H_b in $H(t)$ will modify the overall phase-space behavior of Q in the vicinity of the critical point in such a way that Eq. (4) is generally not fulfilled [25,26].

To illustrate this, we show in Fig. 2(a) an $M(t)$ trajectory driven by an $H(t)$ sequence that is composed of two different time-dependent field components: a fundamental sinusoidal component with period P and amplitude H_0, and a second component of period $P/2$ and amplitude H_2. Here, we observe that $Q \neq 0$ even if $H_b = 0$ and even if the system is in the regime of the dynamic PM phase. This exemplary case shows that the presence of additional even-order Fourier-field components modifies the phase-space behavior of Q and destroys its expected antisymmetry as a function of H_b. In Fig. 2(b), we represent Q as a function of H_b for several H_2 values and for the same $P/\tau = 19$ ratio, shown in Fig. 2(a), which corresponds seemingly to the dynamic PM phase. Here, we can see that Eq. (4) is only valid for the $H_2 = 0$ case. As $|H_2|$ becomes larger, Q deviates ever more from the purely antisymmetric behavior.

In this context, we recently observed that the expected time-reversal symmetry of the dynamic phase space can be restored upon properly defining a renormalized conjugate field H^* [26]. The definition of H^* allows one to recover the time-reversal symmetry in the entire phase space, given that we use the symmetry itself to implicitly define H^*, namely

$$Q(P, H^*) = -Q(P, -H^*). \tag{5}$$

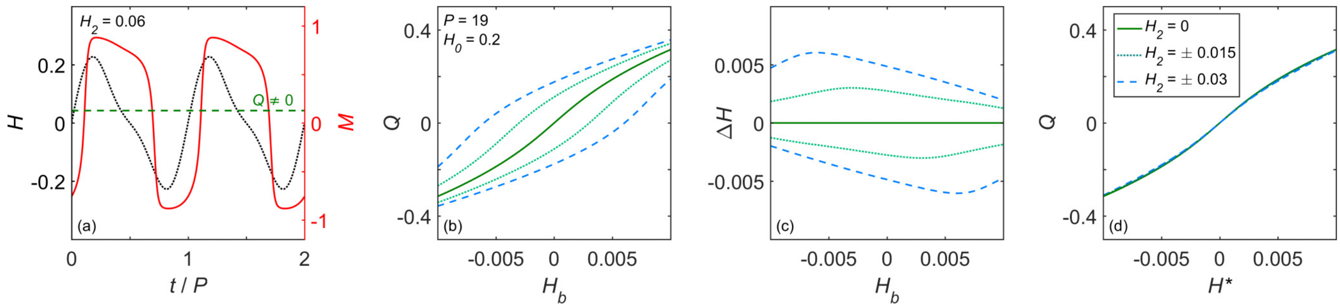

FIG. 2. (a) $M(t)$ behavior, shown as a solid red line, in the presence of $H(t)$, displayed as dotted black line, with $H_0 = 0.2$ and $H_2 = 0.06$. (b) Q vs H_b behavior corresponding to the dynamic PM phase, with $P/\tau = 19$, for several $H_2 = 0, \pm 0.015$, and ± 0.03. (c) ΔH as a function of H_b calculated using Eq. (11) for the cases in (b), with $P/\tau = 19$, and representing the bias correction required to restore time-reversal symmetry. (d) Q represented as a function of H^* showing the restored antisymmetry of the Q vs H^* dependency from (b) and (c). The legend in (d) applies to (b)–(d).

In the absence of even $H(t)$ Fourier components, H^* is just identical to H_b and, thus, Eq. (4) is restored. In the presence of even Fourier components, however, H^* will become a nonlinear superposition of the different components. This definition of a generalized H^* is, in principle, applicable to arbitrary field sequences [26].

It is relevant to note that in the presence of an H_2 component, the scaling relations of Eqs. (2) and (3) cannot be valid as a function of the conventional conjugate field H_b. However, given that H^* represents the conjugate field of Q, and given that the time-reversal symmetry of Eq. (5) is restored, the scaling behaviors of Q in the vicinity of P_c might be restored as well. This general scaling behavior of the DPT based upon the generally applicable and formal definition of H^* according to Eq. (5) has not been investigated or verified to date. On the one hand, this is because most theoretical works until now have been focused on the subspace of half-wave antisymmetric field sequences and, thus, the much broader parameter space of more general field sequences remains largely unexplored. On the other hand, the phase-space behavior of Q near the DPT is known to be substantially modified if compared to the TPT. In the vicinity of the DPT, Q can exhibit rather steep changes as a function of H_b in regions of the PM phase [30]. These so-called metamagnetic anomalies, observed both experimentally [31–33] and theoretically [34–37], constrain the critical regime of Q to a rather narrow parameter space, which has to be much more carefully accessed in the case of DPTs than is necessary in the case of TPTs [27].

Correspondingly, in this work, we investigate whether the use of a generalized conjugate field H^* for general field sequences $H(t)$ that do not necessarily fulfill the half-wave antisymmetry preserves the scaling relations of Eqs. (2) and (3) upon using H^* instead of H_b. For this purpose, we conduct mean-field approximation (MFA) calculations of the phase-space behavior of Q in the vicinity of the critical point for more general subsets of $H(t)$ sequences. In Sec. II of this work, we present the technical aspects of our mean-field theory and the subsequent calculations. Afterwards, we present the key aspects of the definition and characteristics of the generalized conjugate field H^* in Sec. III. In Sec. IV, we show the results of our MFA calculations and perform a scaling analysis of these results to verify the scaling relation and determine the corresponding critical exponents. Finally, we summarize all key results of the present work and give an outlook in Sec. V of this paper.

II. METHODS

The observation of the SOPT for the DPT was originally explored in the context of the MFA of the kinetic Ising model with spin-½ systems, and considering Glauber stochastic dynamics [12,17]. Under these conditions, the time-dependent magnetization behavior $M(t)$, normalized to the low-temperature saturation magnetization M_s, satisfies the following equation:

$$\tau \frac{dM}{dt} = -M(t) + tanh\left(\frac{1}{\mathrm{T}} H_{\mathrm{eff}}(\mathrm{t})\right). \qquad (6)$$

Here, T represents the temperature, normalized to T_C, and $H_{\mathrm{eff}}(t)$ represents the dimensionless effective field acting upon the spins in the system. Specifically, $H_{\mathrm{eff}}(t)$ is given as

$$H_{\mathrm{eff}}(t) = H(t) + H_{\mathrm{MF}}(t), \qquad (7)$$

where $H(t)$ is the dimensionless externally applied magnetic field, normalized to NJ, with N being the number of nearest neighbors. $H_{\mathrm{MF}}(t)$ is the effective mean field, which for bulk systems is $H_{\mathrm{MF}}(t) = M(t)$. In this work, Eq. (6) is numerically integrated using discrete time steps with a time resolution of $P/500$. We self-consistently evaluate $M(t)$ until convergence is achieved. The convergence criterion used in this work is such that the maximum error between the ith iteration of the magnetization trajectory $M_i(t)$ and $M_{i+1}(t)$ is smaller than 10^{-10} for all t. In other words,

$$\max[M_{i+1}(t) - M_i(t)] < 10^{-10}. \qquad (8)$$

Further details regarding the numerical evaluation of (6) can be found elsewhere [13,19,23].

Throughout this work, we only consider $T = 0.8$ for the value of the normalized temperature to make sure that we are restricting ourselves to a parameter space, in which the MFA generates results that are qualitatively similar to those obtained by more accurate techniques, such as Monte Carlo simulations [37,38].

For the present study, we consider a time-dependent external magnetic field,

$$H(t) = H_b + H_0 \sin\left(\frac{2\pi t}{P}\right) + H_2 \sin\left(\frac{4\pi t}{P}\right), \qquad (9)$$

where the first and second terms are the constant bias field and the simple sinusoidal-field sequences, respectively. The third term corresponds to a second-order Fourier component of period $P/2$ which induces an additional asymmetry to the overall $H(t)$ sequence. This H_2 term is the lowest-order even Fourier component, other than H_b, that breaks the half-wave asymmetry in $H(t)$. While higher-order even Fourier components could have been considered as well for this purpose, they do not add another qualitative change to the field sequence as far as their overall symmetry is concerned. Furthermore, higher-order terms are generally less effective in generating magnetization dynamics, given that lower periods of the applied field generally lead to lower responses because they become comparable to the relaxation time constant. Accordingly, we restrict ourselves to a sufficiently small, but meaningful, parameter space. Higher-order odd Fourier components could have been considered as well. However, these do not contribute to breaking the half-wave asymmetry of $H(t)$. This is well known from Monte Carlo simulations using squarelike $H(t)$ sequences, which are formally composed of an infinite sum of odd Fourier components of decreasing magnitude [15,22,25].

The dynamic order parameter is numerically integrated from the obtained $M(t)$ trajectories using Eq. (1). Then, we systematically evaluate Q in the entire (P, H_b) phase space in the vicinity of the critical point and for different H_2 values. Previous works have shown that one can either vary P or H_0 to go through the relevant portion of the dynamic phase space and the SOPT [13,26,32]. Here, we fix the field amplitude H_0 and vary P near P_c to facilitate the scaling analysis according to Eqs. (2) and (3). For a fixed P value, we calculate Q for different H_b such that we map the entire phase space in the vicinity of the SOPT and, at the same time, access the bistability regime of the dynamic FM phase.

III. DEFINITION OF THE GENERALIZED CONJUGATE FIELD

As we have observed in Sec. I in conjunction with Figs. 2(a) and 2(b), the presence of a nonzero H_2 Fourier component leads to a modification of the phase-space behavior of Q such that the H_b-based time-reversal symmetry according to Eq. (4) is not preserved. More specifically, in Fig. 2(b) we observe that for larger opposite H_2 values, the curves seem to become increasingly asymmetric.

The antisymmetry can be restored upon utilizing the H^* axis and considering a nonlinear effective bias-field correction ΔH, such that

$$H^* = H_b + \Delta H. \qquad (10)$$

Such a ΔH bias-field correction can be computed as

$$\Delta H = -\tfrac{1}{2}[H_b(Q) + H_b(-Q)], \qquad (11)$$

where Q depends implicitly on H_b and H_2 [26]. Figure 2(c) shows the ΔH vs H_b behavior for the specific cases shown in Fig. 2(b). Here, we observe that ΔH becomes increasingly relevant for larger $|H_2|$ values and exhibits opposite tendencies for opposite H_2 signs. Figure 2(d) shows the Q values of Fig. 2(b) along the H^* axis, which we calculated by means of Eq. (10). Here, we observe a restored antisymmetry of the dynamic phase-space behavior of Q for all H_2 cases such that all the lines lie essentially on top of each other. The small differences between lines are associated with the fact that the presence of a nonvanishing H_2 modifies P_c and consequently the actual P/P_c ratios are not identical for the different curves shown in Fig. 2(d), as we will discuss in detail in the next section. It is worthwhile to mention that our procedure is widely applicable to nearly any $Q(P, H_b)$ data, because the construction of $\Delta H(P, H_b)$ does not depend on the knowledge of $H(t)$. However, we have to implicitly assume that all field components other than H_b are identical throughout the phase space, so that the (P, H_b) plane is indeed an adequate phase-space representation.

The results of Fig. 2 are obtained for a single P value in the dynamic PM phase. However, the definition of H^* is formally valid for the entire dynamic phase space and can be used accordingly. Figure 3 shows, in several color-coded maps, the entire phase-space behavior of Q for different H_2 values and $H_0 = 0.2$. The calculated datasets here utilize a step size of better than 6.3×10^{-3} in the P axis and 7×10^{-6} in the H_b axis. The step size in H_b is chosen to be much smaller than in P because the accuracy of the ΔH calculations relies heavily on having a sufficiently high H_b resolution in the entire dynamic phase space. Specifically, Fig. 3(c) shows the phase-space behavior of $Q(P, H_b)$ for $H_2 = 0$. Here, we observe the expected antisymmetry as a function of H_b, as well as the occurrence of both dynamic PM and FM phases, as described in conjunction with Fig. 1(d). The FOPT occurs at $H_b = 0$, as expected. In the different maps of Figs. 3(a)–3(e), we observe increasing deviations from the ideal antisymmetric behavior as a function of H_2. First, the line corresponding to the FOPT, which separates equivalent stable states in the dynamic FM phase, shifts relevantly for increasing $|H_2|$ values [39]. On the other hand, the dynamic PM phase is observed to gradually change as well such that on the $H_b = 0$ line, Q increases or decreases with H_2.

Figures 3(f)–3(j) show the bias-field correction $\Delta H(P, H_b)$ data according to Eq. (10) as color-coded maps for the cases of Figs. 3(a)–3(e) right above them. First, in Fig. 3(h) we note that $\Delta H = 0$ in the entire phase space, as expected, given that $H_2 = 0$ and the phase-space behavior of Q is antisymmetric as a function of H_b alone. In the different maps, we observe that the required field corrections $\Delta H(P, H_b)$ become more significant in the dynamic PM phase and increasingly larger for increasing $|H_2|$, as already discussed in conjunction with Fig. 2.

Figures 3(k)–3(o) now show color-coded maps of the phase-space behavior of Q in the (P, H^*) phase space. Along the H^* axis, we observe that antisymmetry is fully restored in all cases, making the color-coded maps virtually identical to each other. This is true even in cases in which H_2 becomes significantly larger than H_b. The figures also verify that the FOPT occurs along the $H^* = 0$ line as it should for a properly defined conjugate field. Thus, our definition of the generalized conjugate field is valid for all points in the dynamic phase

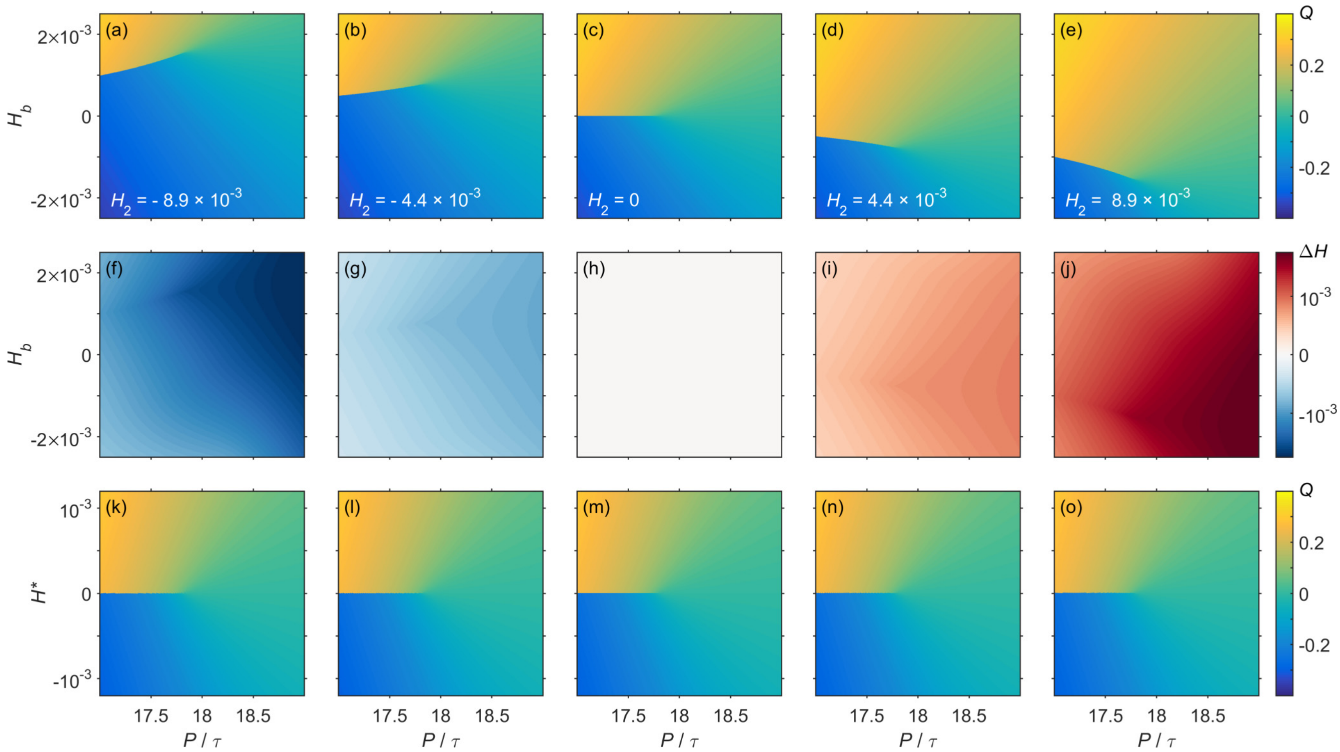

FIG. 3. (a)–(e) Color-coded maps of the phase-space behavior of $Q(P, H_b)$ in the vicinity of P_c for the H_2 values listed in each subfigure. (f)–(j) Color-coded maps of ΔH in the (P, H_b) phase space for the cases shown in (a)–(e) and calculated by utilizing Eq. (11). (k)–(o) Color-coded maps of the $Q(P, H^*)$ phase-space behavior for the same parameters utilized in (a)–(e) and showing the restored antisymmetry upon utilizing the proper bias-field corrections, shown in (f)–(j) The color bars displayed on the right-hand side of (e), (j) and (o) apply to the entirety of each row.

space, and applicable for any given H_2 value such that the time-reversal symmetry is completely restored.

IV. SCALING ANALYSIS

Given our definition of H^* as the conjugate field of Q, which enabled us to restore time-reversal symmetry, we now want to verify if the scaling of Eqs. (2) and (3) is preserved in the (P, H^*) phase space near the critical point for all those field sequences that lack half-wave antisymmetry. For this purpose, we now have to formally rewrite Eq. (3) as

$$Q \propto H^{*1/\delta} \quad \text{for } P = P_c. \tag{12}$$

In order to simultaneously verify that Eqs. (2) and (12) are indeed accurate, we utilize the analogy of the DPT with the TPT. In the case of TPTs, the scaling behavior of $M(T, H)$ near T_C led to the postulation of the Arrott-Noakes equation of state, given as [40]

$$T = T_C + T_1\left[\left(\frac{H}{M}\right)^{1/\gamma} - \left(\frac{M}{M_1}\right)^{1/\beta}\right], \tag{13}$$

where β and γ are the thermodynamic equilibrium critical exponents, from which $\delta = 1 + \gamma/\beta$ can be extracted and M_1, T_1 are material-specific constants. Equation (13) encompasses the scaling behavior of the equilibrium magnetization M as a function of temperature T and field H in the vicinity of the Curie temperature T_C, and has been employed and confirmed in a wide variety of ferromagnetic systems to investigate their equilibrium critical exponents and universality [41–44].

Based on the previously documented equivalence between the scaling behavior of M and Q in the TPT and DPT, respectively, we now assume that data near the DPT follow the dynamic equivalent of the Arrott-Noakes equation, namely,

$$P = P_c + P_1\left[\left(\frac{H^*}{Q}\right)^{1/\gamma} - \left(\frac{Q}{Q_1}\right)^{1/\beta}\right]. \tag{14}$$

Here as well, P_1 and Q_1 are material-specific constants. This expression is formally identical to Eq. (13) and encompasses both scaling behaviors described by Eqs. (2) and (12). This equation of state was recently verified experimentally in ultrathin Co $(10\bar{1}0)$ films and allowed for an accurate quantification of the dynamic critical exponents of this material system [27].

Following this assumption, we now conduct least-squares fits to Eq. (14) for each of the individual $Q(P, H^*)$ maps that we have computed. Given that the dynamic Arrott-Noakes equation of state is a transcendental equation in Q, we fit our datasets as $P(Q, H^*)$ rather than $Q(P, H^*)$, as already indicated by the formulation of Eq. (14). The critical regime for the fit is chosen to encompass a phase-space range of

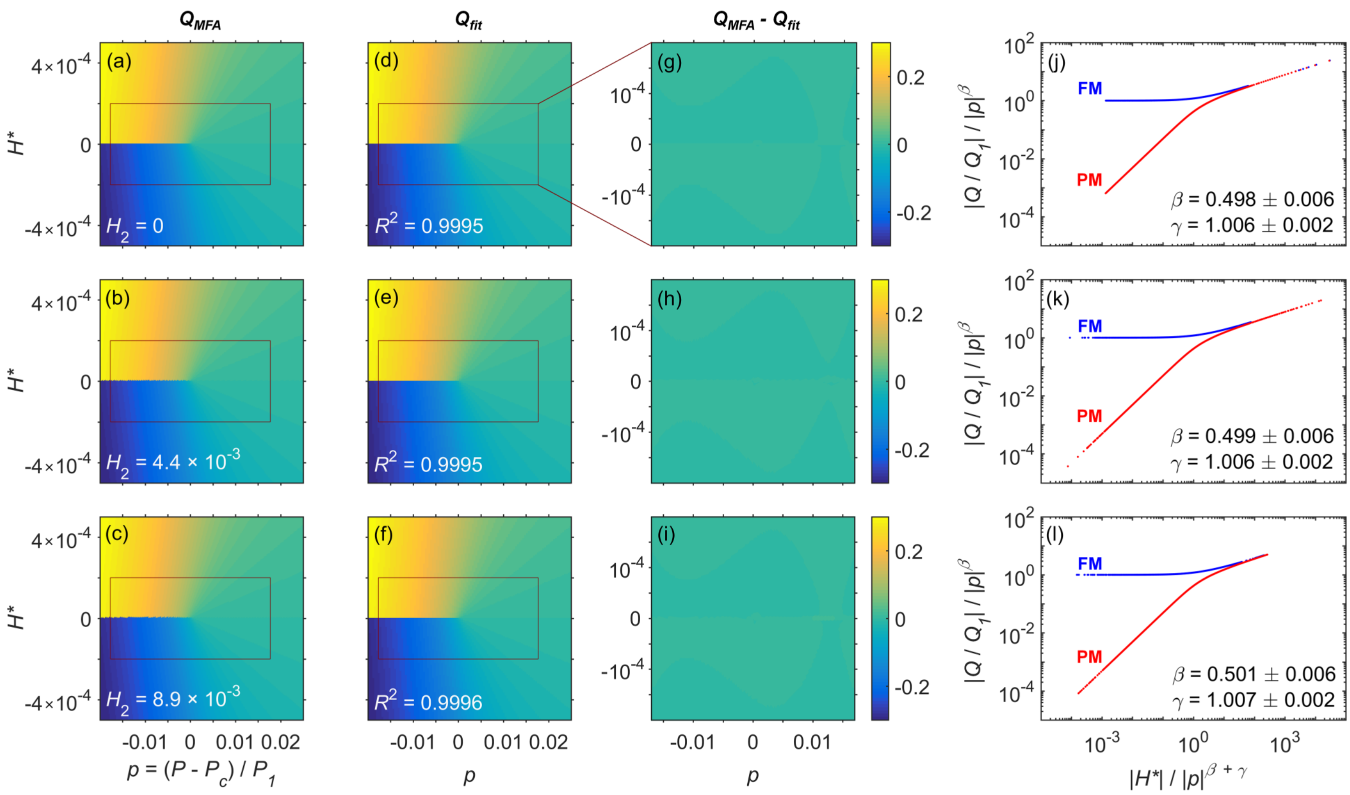

FIG. 4. (a)–(c) Color-coded maps of the phase-space behavior of the dynamic order parameter $Q(P, H^*)$ for several selected values of $H_2 = 0$, 4.4×10^{-3}, and 8.9×10^{-3}. The dark-red rectangles represent the phase-space region selected for our scaling analysis. (d)–(f) Color-coded maps representing the results of the least-squares fits of the $Q(P, H^*)$ data in (a)–(c) inside the dark-red rectangle regions to Eq. (14). (g)-(i) Color maps showing the residual differences between MFA calculations (a)-(c) and least-squares fits (d)–(f) showing negligible systematic deviations in the analyzed critical region. The color bars on the right-hand side of (g)–(i) apply to each entire row. (j)–(l) Arrott plot representation of the renormalized order parameter $|Q|/|p|^\beta$ from (a)–(c) as a function of the renormalized conjugate field $|H^*|/|p|^{\beta+\gamma}$. The blue and red points represent data in the FM and PM phase, respectively. The critical exponents resulting from our analysis are shown in (j)–(l).

$\pm5\%$ of P_c in the P axis and $\pm0.1\%$ of H_0 in the H^* axis, utilizing more than 10^4 computed data points for each individual map. In Fig. 4, we represent the results of this analysis for three exemplarily chosen H_2 values as color-coded maps. Figures 4(a)–4(c) show the MFA calculations of the $Q(P, H^*)$ behavior for three H_2 values as color-coded maps. The regions inside the dark-red rectangle represent the critical regimes selected for our analysis.

Figures 4(d)–4(f) show the resulting least-squares fits of the data in Figs. 4(a)–4(c) to Eq. (14). Here, we observe that the results from the fits, conducted in the region inside the dark-red rectangle only, clearly follow the MFA calculations, with a determination coefficient $R^2 > 0.9990$ for the cases shown here. Furthermore, the fits also reproduce accurately the behavior of the MFA calculations outside the selected scaling regime, implying that our description of Eq. (14) is quantitatively correct in a significantly larger phase-space range than what we utilized here for our scaling analysis. The excellent quality of the fits is also visible in Figs. 4(g)–4(i), where we represent the residual differences between MFA $Q(P, H^*)$ calculations and their corresponding fits to Eq. (14) [45]. Here, we obtain essentially zero systematic deviations in the entire analyzed critical regime, further verifying the validity of our results and data analysis approach.

If scaling is preserved in the analyzed critical regime, then all the data should collapse onto only two curves when the renormalized order parameter $|Q|/|p|^\beta$ is plotted versus the renormalized conjugate field $|H^*|/|p|^{\beta+\gamma}$, with p being the reduced period $p = (P\text{–}P_c)/P_1$. These plots are shown in Figs. 4(j)–4(l) for the datasets displayed and analyzed here [40]. Indeed, we observe here that all the data collapse onto two separate lines, which correspond to the points of the dynamic PM and FM phases. Furthermore, it is important to mention that this scaling is preserved over more than 5 orders of magnitude in both axes, which illustrates the quantitative relevance and precision of our study here.

These results verify that scaling is present in all cases upon utilizing H^* as the proper conjugate field. Furthermore, our analysis reports critical exponents $\beta = 0.5 \pm 0.006$ and $\gamma = 1.006 \pm 0.002$, leading to $\delta = 3.012 \pm 0.020$, which fully agree with the critical exponents of the conventional mean-field model [24,46].

We have repeated this entire analysis for a large number of H_2 values. In Fig. 5(a), we show in blue the obtained

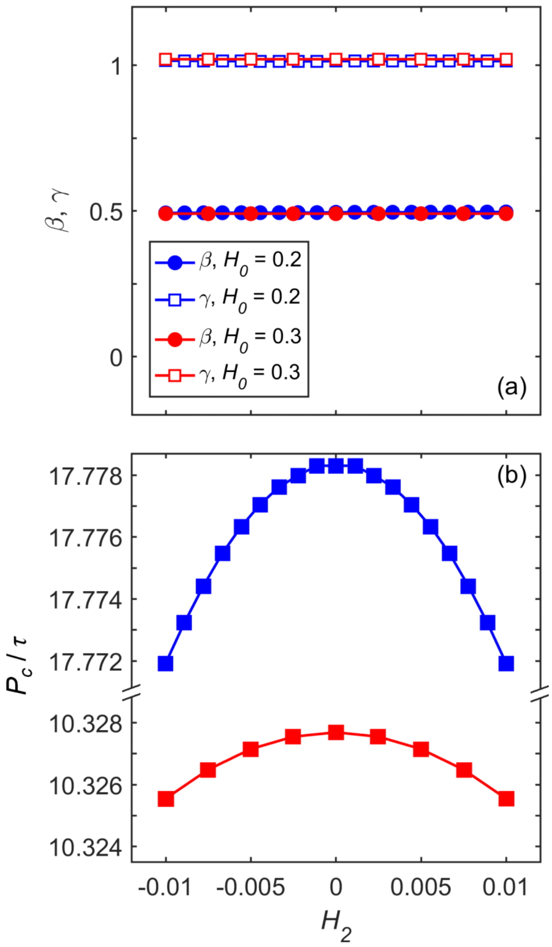

FIG. 5. (a) Critical exponents β (filled circles) and γ (squares) extracted from the least-squares fits of our numerical $Q(P, H^*)$ datasets to Eq. (14) represented as a function of H_2 for $T = 0.8$. Data for two different $H_0 = 0.2$ (blue) and 0.3 (red) are shown as indicated in the legend. (b) P_c as a function of H_2 for the two different H_0 values displayed in (a), utilizing the same color code for identification.

critical exponents for many different H_2 values and $H_0 = 0.2$. The exponents remain essentially constant in the entire analyzed H_2 range, with a maximum deviation of 0.008 for β and 0.02 for γ. In Fig. 5(b), we represent the critical period P_c as a function of H_2. Here, we observe that P_c exhibits a quadratic behavior as a function of H_2, as already mentioned in conjunction with Fig. 2(d) [26]. This trend originates from the fact that a linear combination of first- and second-order Fourier components increases the effective field amplitude, which leads to a reduction of P_c [13]. Interestingly, the addition of H_2 in the field sequence only affects the actual position of P_c and only in a very modest way, while the rest of the fit parameters remain all essentially constant.

In order to further demonstrate the validity of our results, we repeated our entire analysis for $H_0 = 0.3$, and the corresponding results are shown in red in Fig. 5. In Fig. 5(a), we observe that both β and γ are fundamentally identical to the values obtained for the case with $H_0 = 0.2$. In Fig. 5(b), P_c still exhibits the expected quadratic behavior. However, now, lower P_c values are obtained for the larger H_0 value, because larger field amplitudes expand the stability range of the dynamic PM phase and shift the critical point accordingly [13].

In all the cases of our study here, R^2 is found to be larger than 0.9983, which is an excellent indication that the scaling behavior is fully preserved in the entire analyzed parameter space and for all the different field sequences. Furthermore, the critical exponents correspond to those of the mean-field Ising model, verifying the fact that universality is preserved as well, once one considers the proper H^* as conjugate field. Given these findings, all our results validate our approach to determine the generalized conjugate field H^* as the true conjugate field of the order parameter Q when arbitrary $H(t)$ field sequences are considered. The here-obtained results also valildate the dynamic Arrott-Noakes equation of state in the vicinity of the critical point, which was only recently postulated for the purpose of analyzing experimental data [27].

V. CONCLUSIONS AND OUTLOOK

In this work, we verify that the scaling behavior of the dynamic order parameter Q in the vicinity of the DPT is preserved as a function of a generalized conjugate field H^* and the field period P for magnetic-field sequences that drive the dynamic state of the system even if they do not exhibit half-wave antisymmetry. This aspect validates our specific definition and computation scheme for H^* as generating the true conjugate field of the dynamic order parameter Q. Furthermore, our mean-field analysis of Q in the vicinity of the DPT results in dynamic critical exponents that are identical in all cases and are also in full agreement with the symmetry class of the mean-field model, and more generally verify the concept of universality. This is true even if the system is subject to magnetic-field sequences that are strongly asymmetric with large amplitudes of a second-order Fourier component.

More generally, our study here shows that for a wide range of field-sequence modifications one can recover the critical behavior and corresponding scaling relations of the dynamic order parameter in a system with seemingly broken symmetries upon defining a suitable renormalized phase-space coordinate system. However, we need to realize that this does not necessarily have to be the case in all possible scenarios. For instance, if the field-sequence modifications that generate the broken symmetries also change the phase transition from continuous to discontinuous, a renormalized recovery of critical behavior should not be possible anymore. This scenario might actually occur within the mean-field model of the DPT at sufficiently low temperatures [12,23], but is a subject that goes beyond the scope of the present work.

Finally, our work shows that the recently postulated dynamic Arrott-Noakes equation of state describes the critical behavior of the dynamic order parameter Q most accurately, even in strongly asymmetric magnetic-field sequences. Therefore, this work constitutes a theoretical utilization and verification of this equation-of-state approach and analysis.

In the future, it would be relevant to investigate the validity of both the dynamic Arrott-Noakes equation of state and the generalized conjugate field as the true conjugate field of Q in the context of more precise theoretical schemes, which could be achieved, for example, by means of Monte Carlo simulations. Hereby, such computational schemes should allow for a dimensionality analysis by taking the actual dimensionality of the order parameter, as well as the lattice, into consideration, which is not accessible in our mean-field approach here. Also, it would be interesting to explore the validity of our definition of H^* in the context of more complex and/or arbitrary magnetic-field sequences either experimentally or theoretically, which could be composed of higher-order even and odd Fourier components.

ACKNOWLEDGMENTS

The authors acknowledge E. Vatansever for his valuable comments on the manuscript. We acknowledge support by the Spanish Ministry of Science and Innovation under the Maria de Maeztu Units of Excellence Programme (Grant No. CEX2020-001038-M), Project No. PID2021-123943NB-I00 (OPTOMETAMAG), as well as the support received by Predoctoral Fellowship No. PRE2019-088428.

[1] M. C. Cross and P. C. Hohenberg, Rev. Mod. Phys. **65**, 851 (1993).

[2] M. Henken, H. Hinrichsen, and S. Lübeck, *Non-Equilibrium Phase Transitions: Volume 1: Absorbing Phase Transitions (Theoretical and Mathematical Physics)* (Springer, USA, 2008).

[3] P. H. Kes, N. Kokubo, and R. Besseling, Physica C **408-410**, 478 (2004).

[4] M. Benkraouda, I. M. Obaidat, U. Al. Khawaja, and N. M. J. Mulaa, Supercond. Sci. Technol. **19**, 368 (2006).

[5] V. K. Jirsa and H. Haken, Phys. Rev. Lett. **77**, 960 (1996).

[6] N. Ogawa, Y. Murakami, and K. Miyano, Phys. Rev. B **65**, 155107 (2002).

[7] D. Bonamy, S. Santucci, and L. Ponson, Phys. Rev. Lett. **101**, 045501 (2008).

[8] M. Heyl, A. Polkovnikov, and S. Kehrein, Phys. Rev. Lett. **110**, 135704 (2013).

[9] S. Vajna and B. Dóra, Phys. Rev. B **89**, 161105(R) (2014).

[10] A. L. Stella, A. Chechkin, and G. Teza, Phys. Rev. Lett. **130**, 207104 (2023).

[11] A. L. Stella, A. Chechkin, and G. Teza, Phys. Rev. E **107**, 054118 (2023).

[12] T. Tomé and M. J. de Oliveira, Phys. Rev. A **41**, 4251 (1990).

[13] P. Riego, P. Vavassori, and A. Berger, Physica B **549**, 13 (2018).

[14] B. K. Chakrabarti and M. Acharyya, Rev. Mod. Phys. **71**, 847 (1999).

[15] G. M. Buendía and P. A. Rikvold, Phys. Rev. E **78**, 051108 (2008).

[16] Y. Yüksel and E. Vatansever, J. Phys. D: Appl. Phys. **55**, 073002 (2022).

[17] R. J. Glauber, J. Math. Phys. **4**, 294 (1963).

[18] The trajectories are obtained using the mean-field approximation (MFA) that is described in Methods, Sec. II of this work.

[19] A. Berger, O. Idigoras, and P. Vavassori, Phys. Rev. Lett. **111**, 190602 (2013).

[20] S. W. Sides, P. A. Rikvold, and M. A. Novotny, Phys. Rev. Lett. **81**, 834 (1998).

[21] S. W. Sides, P. A. Rikvold, and M. A. Novotny, Phys. Rev. E **59**, 2710 (1999).

[22] G. Korniss, C. J. White, P. A. Rikvold, and M. A. Novotny, Phys. Rev. E **63**, 016120 (2000).

[23] R. A. Gallardo, O. Idigoras, P. Landeros, and A. Berger, Phys. Rev. E **86**, 051101 (2012).

[24] D. T. Robb, Y. H. Xu, O. Hellwig, J. McCord, A. Berger, M. A. Novotny, and P. A. Rikvold, Phys. Rev. B **78**, 134422 (2008).

[25] D. T. Robb and A. Ostrander, Phys. Rev. E **89**, 022114 (2014).

[26] M. Quintana and A. Berger, Phys. Rev. E **104**, 044125 (2021).

[27] M. Quintana and A. Berger, Phys. Rev. Lett. **131**, 116701 (2023).

[28] C. M. Valderrama, M. Quintana, A. Martínez-de-Guerenu, T. Yamauchi, Y. Hamada, Y. Kurokawa, H. Yuasa, and A. Berger, J. Phys. D: Appl. Phys. **54**, 435002 (2021).

[29] C. M. Valderrama, M. Quintana, A. Martínez-de-Guerenu, T. Yamauchi, Y. Hamada, Y. Kurokawa, H. Yuasa, and A. Berger, J. Phys. D: Appl. Phys. **55**, 435007 (2022).

[30] P. Riego, P. Vavassori, and A. Berger, Phys. Rev. Lett. **118**, 117202 (2017).

[31] J. M. Marín Ramírez, E. Oblak, P. Riego, G. Campillo, J. Osorio, O. Arnache, and A. Berger, Phys. Rev. E **102**, 022804 (2020).

[32] M. Quintana, E. Oblak, J. M. Marín Ramírez, and A. Berger, Phys. Rev. B **102**, 094436 (2020).

[33] M. Quintana, C. Martín Valderrama, and A. Berger, Phys. Rev. E **108**, 064121 (2023).

[34] X. Shi and P. Liu, Physica A **536**, 120998 (2019).

[35] Y. Yüksel, Phys. Rev. E **108**, 034125 (2023).

[36] Y. Yüksel, Physica A **580**, 126172 (2021).

[37] G. Berkolaiko and M. Grinfeld, Phys. Rev. E **76**, 061110 (2007).

[38] G. M. Buendía and P. A. Rikvold, Phys. Rev. B **96**, 134306 (2017).

[39] The FOPT and subsequently the stable states of Q are determined by the $H^* = 0$ condition in the entire dynamic FM phase.

[40] A. Arrott and J. E. Noakes, Phys. Rev. Lett. **19**, 786 (1967).

[41] K. Miyatani and K. Yoshikawa, J. Appl. Phys. **41**, 1272 (1970).

[42] H. Hiroyoshi, A. Hoshi, and Y. Nakagawa, J. Appl. Phys. **53**, 2453 (1982).

[43] K. Ghosh, C. J. Lobb, R. L. Greene, S. G. Karabashev, D. A. Shulyatev, A. A. Arsenov, and Y. Mukovskii, Phys. Rev. Lett. **81**, 4740 (1998).

[44] D. Fuchs, M. Wissinger, J. Schmalian, C.-L. Huang, R. Fromknecht, R. Schneider, and H. v. Löhneysen, Phys. Rev. B **89**, 174405 (2014).

[45] The residual differences are obtained by error propagation of Eq. (14).

[46] O. Idigoras, P. Vavassori, and A. Berger, Physica B **407**, 1377 (2012).

Correction: The legend of the previously published Fig. 2(d) contained a minor error and has been replaced. The caption to Fig. 5 contained a typographical error and has been fixed.

Second Correction: A typographical error in Eq. (11) has been fixed.